ADVANCED ENERGY MATERIALS

www.advenergymat.de

A Soft and Robust Spring Based Triboelectric Nanogenerator for Harvesting Arbitrary Directional Vibration Energy and Self-Powered Vibration Sensing

*Minyi Xu, Peihong Wang, Yi-Cheng Wang, Steven L. Zhang, Aurelia Chi Wang, Chunli Zhang, Zhengjun Wang, Xinxiang Pan, and Zhong Lin Wang**

Vibration is a common mechanical phenomenon and possesses mechanical energy in ambient environment, which can serve as a sustainable source of power for equipment and devices if it can be effectively collected. In the present work, a novel soft and robust triboelectric nanogenerator (TENG) made of a silicone rubber-spring helical structure with nanocomposite-based elastomeric electrodes is proposed. Such a spring based TENG (S-TENG) structure operates in the contact-separation mode upon vibrating and can effectively convert mechanical energy from ambient excitation into electrical energy. The two fundamental vibration modes resulting from the vertical and horizontal excitation are analyzed theoretically, numerically, and experimentally. Under the resonant states of the S-TENG, its peak power density is found to be 240 and 45 mW m^{-2} with an external load of 10 MΩ and an acceleration amplitude of 23 m s^{-2}. Additionally, the dependence of the S-TENG's output signal on the ambient excitation can be used as a prime self-powered active vibration sensor that can be applied to monitor the acceleration and frequency of the ambient excitation. Therefore, the newly designed S-TENG has a great potential in harvesting arbitrary directional vibration energy and serving as a self-powered vibration sensor.

1. Introduction

Vibration is a common mechanical phenomenon in our daily life; for example, it is present in engines, aircrafts, bridges, buildings, etc. The omnipresent vibration can also serve as a source of energy to power self-powered systems, such as micro-electromechanical systems, remote environmental sensors, homeland security, and even portable/wearable personal electronics.[1] Triboelectric nanogenerators (TENGs), are able to generate electrical output based on contact triboelectrification and electrostatic induction in response to an external mechanical stimuli.[2] Its fundamental physics and output characteristics can be attributed to Maxwell's displacement current.[3] Additionally, it is a cost-effective, simple, and robust technique for energy harvesting,[1,4–18] and can alternatively serve as an active mechanical motion sensor using its own electrical output without a secondary power source.[19–27]

Spring-assisted TENGs are superior for vibration energy harvesting and impact detection at a weak ambient vibration than those without a spring.[5,28–30] For example, Jiang et al.[30] designed a form of spring-assisted TENG for harvesting water wave energy, in which two Cu-PTFE-covered acrylic blocks connected by a spring were placed between two Cu electrodes anchored on two internal walls of a box-like device. Springs store mechanical kinetic energy and potential energy during mechanical triggering for use in subsequent cycles of electricity conversion, transforming low frequency motion into high frequency oscillation, and improving energy harvesting efficiency. The accumulated charge of the spring-assisted TENG increased by 113.0%, and the efficiency improved by 150.3%. Following a similar line, Wu et al.[29] found that integrating a mechanical spring-based amplifier with the ability to amplify both the vibration frequency and amplitude with a TENG improved its low-frequency performance by up to ten times by using the stored potential energy by the spring. Also, Hu et al.[28] installed a contact-separation mode TENG on the front of a suspended 3D helical structure, and used it to harvest wave energy and serve as an active sensor. However, since these aforementioned TENGs were based on hard material (acrylic) attached to

Dr. M. Xu, Dr. P. Wang, Dr. Y.-C. Wang, S. L. Zhang, A. C. Wang, Dr. C. Zhang, Dr. Z. Wang, Prof. Z. L. Wang
School of Materials Science and Engineering
Georgia Institute of Technology
Atlanta, GA 30332-0245, USA
E-mail: zhong.wang@mse.gatech.edu
Dr. M. Xu, Prof. X. Pan
Marine Engineering College
Dalian Maritime University
Dalian 116026, China
Dr. P. Wang
School of Physics and Materials Science
Anhui University
Hefei, Anhui 230601, China
Dr. C. Zhang
Department of Engineering Mechanics
Zhejiang University
Hangzhou, Zhejiang 310027, China
Prof. Z. L. Wang
Beijing Institute of Nanoenergy and Nanosystems
Chinese Academy of Sciences
Beijing 100085, China

DOI: 10.1002/aenm.201702432

one end of a spring, the researchers could only use the vertical or axial spring vibrational mode to harvest vibrations in that direction. Springs also possess a horizontal vibration mode due to the bendable property of the spring and its mass, which has not yet been used in a TENG to harvest horizontally oriented vibration. The integration of a TENG and spring for arbitrary direction vibration energy harvesting is highly desired but remains a great challenge.

Thus, in the present work, we design a TENG integrated with a spring by fabricating a helical structure along the spring wire. The helical structure is composed of two conductive elastomeric layers serving as electrodes and two nonconductive elastomeric (silicone rubber) layers. With the assistance of a wire spring and soft silicone rubber, both vertical and horizontal vibration excitation can alter the distance between the helical structure's adjacent coils and form a contact-separation mode TENG. The two fundamental vibration modes are analyzed by combining theoretical, numerical, and experimental methods. The mechanical properties and electrical output of the spring-based TENG (S-TENG) are measured using a linear motor and a shaker. Additionally, the dependence of the S-TENG's output signal on external vibration indicates that it could be used as a self-powered active sensor to sense the acceleration and frequency of vibration. Therefore, our newly designed S-TENG has great potential applications in harvesting arbitrary vibration energy, such as vehicle vibration, building vibration, and vibration triggered by ocean wave, wind, walking, etc. At the same time, it is also well suited for a self-powered vibration sensor.

2. Results and Discussion

2.1. Structure and Working Principle of S-TENG

Figure 1a,c shows a schematic diagram and a photo of the S-TENG, respectively. A TENG based on the integration of elastomer and spring to form a helical structure was designed. Along the cut surface of the elastomer-spring helical structure, a layer of conductive elastomer topped the surface served as an electrode, and another layer of electrode was placed at the bottom of the helical structure surface covered by another layer of silicone rubber shown in black in Figure 1a. The detailed fabrication processes are described in the Experimental Section and Figure S1 (Supporting Information). The elastomeric electrode is made by mixing well silicone rubber and carbon nanofiber (diameter around 100–200 nm) (Figure 1b), and can be stretched up to the strain of 133%. The carbon nanofiber was used, due to its low cost and good conductivity. The sheet resistance per unit length R of the conductive elastomer is about 160 Ω cm^{-1} without any strain, but the resistance increases about five times at the strain of 133% (Figure S2, Supporting Information). When a silicone rubber layer (with a conductive elastomeric electrode on the back) and an elastomeric electrode layer are forced to contact with each other and then separated, electricity can be generated (30 V in silicone rubber/electrode combination), due to triboelectrifcation and electrostatic induction (more mechanisms will be discussed in the next paragraph). Interestingly, when the elastomeric electrode layer was replaced by another silicone rubber layer, or vice versa, in the same experiments, the

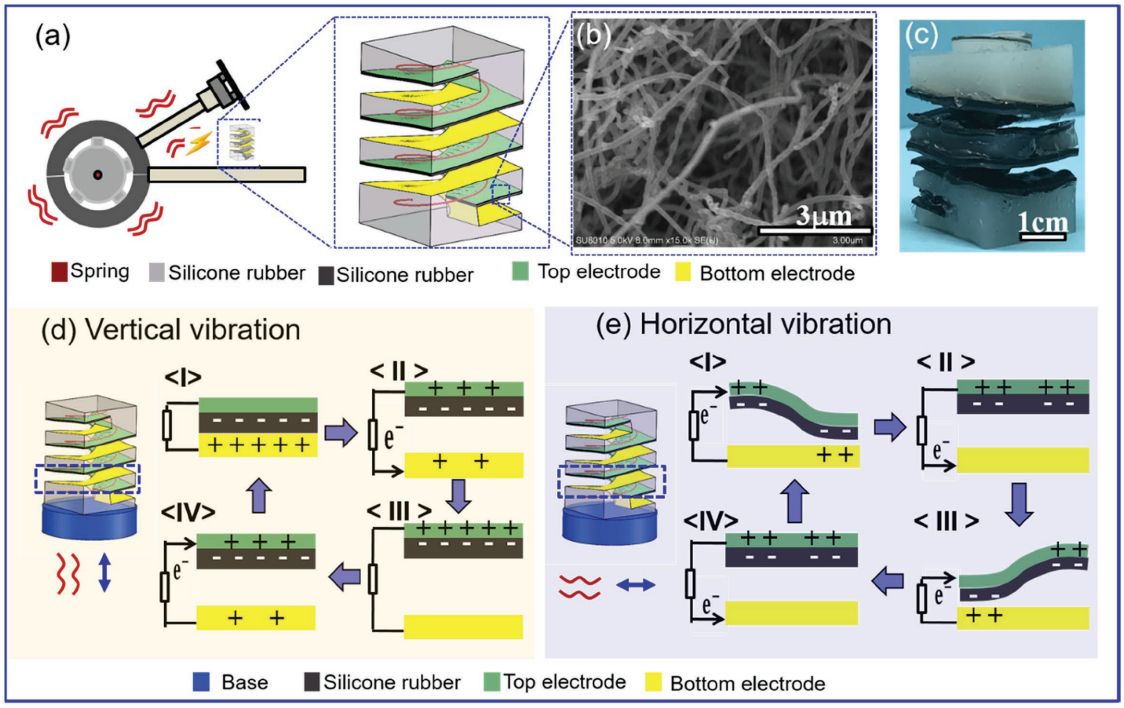

Figure 1. a) The device schematic of the S-TENG. Note that the gray silicone rubber layer containing a spring forms a base on which other layers can be built, and the black silicone rubber layer along with the electrode layer form a contact-separation pair. Both top and bottom electrodes are made of carbon nanofiber-mixed silicone rubber. b) SEM image of the carbon nanofiber for preparing the elastomeric electrode. c) Photo of the as-prepared S-TENG. Working mechanisms of the S-TENG under d) vertical vibration excitation and e) horizontal vibration excitation.

voltage output decreased to 45 times (silicone rubber/silicone rubber) and 150 times (electrode/electrode) lower, respectively (Figure S3, Supporting Information). Since silicone rubber is in the negative part in the triboelectric series,[2] the results suggest that adding carbon-based materials into silicone rubber may result in a more positive elastomeric electrode.

Figure 1d,e shows the working mechanisms of the S-TENG under vertical and horizontal vibration, respectively. The top of the S-TENG is freely able to move, while the bottom is fixed on a base that can vibrate in arbitrary directions. Under external vertical vibration excitation, the distance between a helical structure's adjacent surfaces changes, forming a contact-separation mode TENG,[28] detailed as follows. Electrons are transferred from the elastomeric electrode layer to the silicone rubber layer upon contact, resulting in positive and negative triboelectric charges on elastomeric electrode surface and the silicone layer, respectively (Figure 1d-I). The original contacted surfaces then start to separate, due to the S-TENG oscillation along the vertical direction, triggered by the external vertical vibration (Figure 1d-II). As the separation between the silicone layer and elastomeric electrode layer increases, electrons move from the top electrode layer to the bottom electrode until the separation at a maximum (Figure 1d-III). Then, the spring causes the separation distance to decrease again, as the presence of external vibration, which causes the movement of electrons from the bottom electrode to the top electrode layer (Figure 1d-IV). Thus, a periodical voltage, current, and charge signal can be generated due to the periodic transfer of electrons between two elastomeric electrode layers resulting from S-TENG oscillations in response to mechanical disturbances in the environment.

Under horizontal vibration excitation, the S-TENG's helical structure's adjacent surfaces can contact on one side and separate on the other side, also forming a contact-separation mode TENG. One side (right side in Figure 1e-I) of the soft silicone rubber layer contacts the elastomeric electrode layer, resulting in positive and negative triboelectric charges on the silicone and electrode surface. When the spring oscillates, the distance between two layers increases, resulting in the electrons move from the top electrode layer to the bottom electrode until the spring moves back to the middle state (Figure 1e-II). Furthermore, when the S-TENG oscillates, resulting in a decrease in distance between the other side (left side in Figure 1e-III) of the silicone rubber and electrode, the electrons move from the bottom electrode layer to the top electrode layer until part of the silicone rubber layer contacts the bottom electrode. Similarly, the electrons move from the top electrode layer to the bottom electrode layer when the spring moves to the middle state again (Figure 1e-IV). One of the key reasons that the S-TENG can oscillate horizontally is that with one side of the device is fixed on the base, i.e., vibration source, along with the assistance of the spring and the mass of the device, horizontal oscillation of S-TENG can be achieved. More theoretical discussions will be included in the later section.

According to the theory behind the contact-separation mode TENG, the relationship between the separation distance of two triboelectric charged layers $x(t)$, charge density σ, and the open-circuit voltage V_{OC} is as follows[31]

$$V_{OC} = \frac{\sigma x(t)}{\varepsilon_0} \tag{1}$$

where σ is the charge density of the silicone rubber surface, and ε_0 is the dielectric constant in vacuum. As shown in Equation (1), V_{oc} is proportional to the distance between the two plates, which reaches a maximum when the two layers are separated the farthest (Figure S4, Supporting Information). In addition, V_{oc} is proportional to the triboelectric charges generated on the contacting surface, which depend on the property of the two surfaces and the process of friction. Therefore, the performance of S-TENG can be optimized by choosing proper materials or modified surface morphology to increase charge density, and by designing structure to enhance separation distance. Also, the size and weight of the silicone rubber and the spring's stiffness also affect the resonant frequencies of S-TENG. To tune the device to response to different resonant frequencies, the user could choose various springs with different stiffness, or thickness of silicone rubber, etc. In this work, we selected carbon-based materials, resulting in a positively charged silicone rubber electrode (Figure S3, Supporting Information).

2.2. Performance of S-TENG

After discussing the working mechanisms of S-TENG, we further used a linear motor to characterize the electrical output performance of S-TENG. **Figure 2** shows the mechanical properties and electrical outputs of the S-TENG measured using a linear motor. The S-TENG can be compressed and released periodically by the linear motor shown in Figure 2a. Obviously, the larger the displacement A of compressing or releasing the S-TENG, the larger force or pressure is applied on the S-TENG. However, the relationship between the force and displacement can be divided into two parts (Figure 2b). For a smaller displacement ($A < 10$ mm), the force or pressure increases linearly with displacement (see the inset in Figure 2b), since the spring is compressed elastically before the silicone rubber layer and electrode layer are fully contacted. The slope of such relationship is the elasticity coefficient k of the S-TENG, thus $k = 1.3$ N cm^{-1} for the present S-TENG. With further increase of displacement, the force or pressure increases faster, since the soft silicone rubber begins to be compressed and its elasticity is larger than that of the present spring.

The peak voltage, current, and charge of S-TENG also increase with pressure (Figure 2c–e). This is because higher pressure causes the charge density on the surface of the soft silicone rubber layer to increase.[32] In addition, the voltage, current, and charge signals of the S-TENG are periodic, corresponding to the periodic movement of the linear motor, as shown in the insets in Figure 2c,d. The voltage V_{TENG} of the S-TENG with different loads R is also measured, thus the power density P can be obtained using the relationship $P = V^2_{TENG}/RS$. Here S is the cross-sectional area of the S-TENG, i.e., $S = 3$ cm $\times$ 3 cm = 9 cm^2. The peak power obtained is found to be 180 mW m^{-2} at $R = 100$ MΩ for the displacement of 2 cm and a frequency of 1 Hz.

To further investigate the working mechanisms of the S-TENG, we introduce a theoretical discussion in this section. For the proposed S-TENG, it can be triggered by the vibration of the base from arbitrary directions as mentioned above, we focus our discussions on the behavior of the S-TENG under the

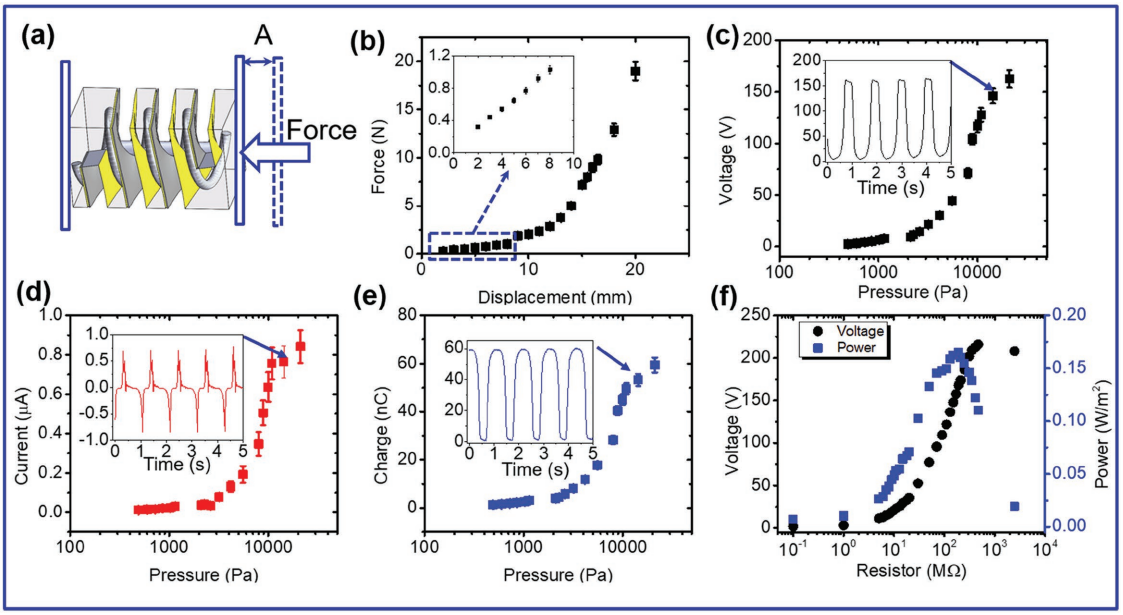

Figure 2. The mechanical properties and electrical output of the S-TENG measured using a linear motor. a) The schematic of S-TENG under compression by linear motor. b) Elastic characteristics of S-TENG. The inset figure demonstrates the linearity of the S-TENG's elasticity with a displacement below 10 mm. c) Peak voltage, d) peak current, and e) peak charge of S-TENG as a function of applied pressure. The inset figures demonstrate the corresponding instantaneous voltage, current, and charge at a pressure of 20 000 Pa. f) Peak voltage and peak power of S-TENG as functions of the load resistance for S-TENG.

vertical and horizontal excitations as two representative samples. Under these two kinds of excitations, the physical model for the proposed S-TENG can be simplified to a single degree-of-freedom (SDOF) oscillator system, as shown in **Figure 3**a, for convenience. For the vertical excitation, the equivalent system consists of an inertial mass m, a spring elasticity coefficient k, and a mechanical damping c. $x(t)$ denotes the displacement of the mass, $x_b(t) = A_b\, e^{i\omega t}$ is the vertical displacement of the base with A_b being the amplitude of base excitation, and the corresponding acceleration $a = -A_b\omega^2 e^{i\omega t}$. Through the Newton's second law of motion, the differential equation governing the vertical vibration of the equivalent spring-mass system for the S-TENG can be described as follows[21,33,34]

$$m\ddot{x}(t) + c\left[\dot{x}(t) - \dot{x}_b(t)\right] + k\left[x(t) - x_b(t)\right] = 0 \quad (2)$$

where $\ddot{x}(t)$ and $\dot{x}(t)$ are the acceleration and velocity of the mass, and $\dot{x}_b(t)$ is the base velocity. For the horizontal excitation, the horizontal movement $y_b(t)$ of the base leads to the bending of the S-TENG, as shown in **Figure 4**a. Assume the deflection angle $\theta(t)$ of the spring to be small, the motion of the S-TENG can be thus treated as an equivalent horizontal vibration of spring-mass-damper system. $y(t)$ denotes the displacement of the mass. Similarly, the equilibrium equation of motion for the S-TENG under the horizontal excitation is written as

$$m\ddot{y}(t) + c_{eh}\left[\dot{y}(t) - \dot{y}_b(t)\right] + k_{eh}\left[y(t) - y_b(t)\right] = 0 \quad (3)$$

Here, k_{eh} and c_{eh} are equivalent horizontal spring stiffness and mechanical damping. k_{eh} is obtained to be 0.5 N cm^{-1} by measuring the force that causes the top layer of the S-TENG to move a certain horizontal displacement. From Equations (2) and (3), the natural frequencies of the S-TENG under the vertical and horizontal vibration excitations can be easily obtained, which are $f_{nv} = (k/m)^{1/2}/2\pi \approx 13$ Hz, and $f_{nh} = (k_{eh}/m)^{1/2}/2\pi \approx 8$ Hz, respectively, using $m = 20$ g and $k = 1.3$ N cm^{-1}, $k_{eh} = 0.5$ N cm^{-1}. The natural frequencies f_{nv} and f_{nh} are consistent with the experimental data, as shown in Figure 3c. It should be noted here that the simplified single degree of freedom spring-mass system only represents one dominated deformation or movement mode of the S-TENG structure under vertical or horizontal excitation. Additionally, to optimize the resonance frequencies of the S-TENG, springs with different stiffness (k, k_{eh}), and the mass m of the silicone rubber could be used. For example, the resonance frequencies increase with high value of spring stiffness or a low value of structure mass, which is correlated to the weight of the silicone rubber.

Finite element simulation for modal analysis of the S-TENG was also performed with ANSYS. In fact, there are many vibrational modes for the 3D S-TENG structures. As the excitation frequency of vibrations from the ambient environment is relatively low, only the first three fundamental modes of the S-TENG correspond to the lowest resonant frequency scenarios were simulated and discussed (Figure 3b).

It can be seen that both the first and second order modes represent the flexural deformations of the S-TENG in the two vertical symmetry planes, and the corresponding natural frequencies are 7.5 and 7.6 Hz, respectively. They agree well with the natural frequency (i.e., $f_{nh} = (k_e/m)^{1/2}/2\pi \approx 8$ Hz) predicted by the SDOF spring-mass-damper model shown in Figure 3a-II. The third mode represents the vertically extensional deformation of the S-TENG, and the corresponding natural frequency is 17 Hz, which also agrees well with the natural frequency (i.e., $f_{np} = (k_e/m)^{1/2}/2\pi \approx 13$ Hz) predicted by

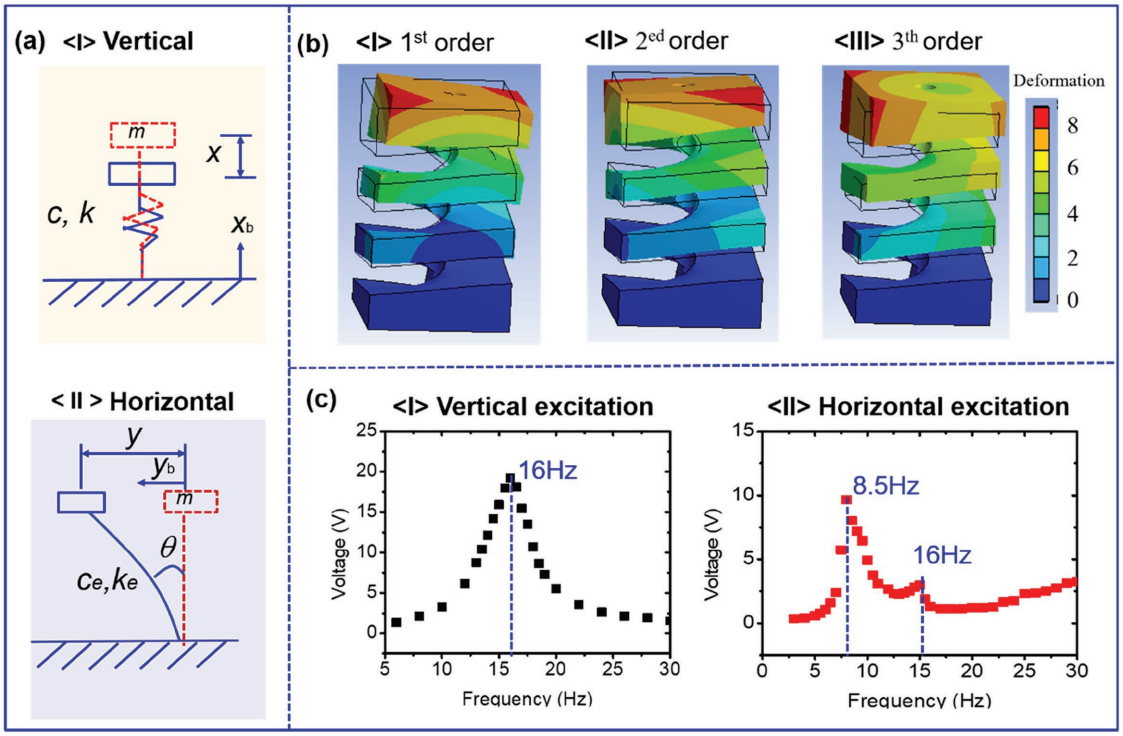

Figure 3. Physical models, modal simulation, and frequency response of the S-TENG. a) Physical models for S-TENG under vertical vibration excitation and horizontal vibration excitation. b) First three vibration modes of the S-TENG simulated by ANSYS software. c) Measured frequency response of the S-TENG under vertical vibration excitation and horizontal vibration excitation.

the SDOF spring-mass-damper model shown in Figure 3a-I. The different mode shapes in the first three order modes lead to a large difference in the frequency response of the S-TENG under different directions of external excitation, which is further verified by the following experimental data.

The frequency response of the S-TENG was tested by putting the S-TENG on an electrodynamic shaker, which provides an external harmonic vibration with controlled amplitude and frequency along the vertical direction. To achieve the horizontal vibration, the shaker was rotated by 90°. Figure 3c shows the frequency response of the S-TENG under the acceleration amplitude $|a| = |A_g\omega^2| = 10$ m s^{-2} and the frequency range of 0–30 Hz. Vibration modes can be stimulated when the external excitation frequency is near structural resonance frequencies. At this moment, the S-TENG can produce a larger electrical power output. As shown in Figure 3c-I, the resonant frequency of the system is observed to be 16 Hz for vertical vibration excitation, which corresponds to the third order mode, i.e., extension deformation of the S-TENG as shown in Figure 3b-III. Under horizontal vibration excitation, the highest electrical signal is obtained at the frequency of 8.5 Hz, which comes from the first and second order vibration modes, i.e., flexural deformation of the S-TENG as indicated in Figure 3b-I,-II. The frequency response near 8.5 Hz of the S-TENG only has one peak due to very similar resonant frequencies and mode shapes of the first and second order modes. It is interesting to note that there is an additional lower voltage peak at a higher frequency (≈16 Hz) in Figure 3c-II. This reveals that the extension deformation (the third vibration mode) of the S-TENG can also be stimulated by the horizontal vibration at its resonance frequency to produce contact-separation motion between silicone rubber layer and conductive electrode layer. Thus, it suggests that the S-TENG can harvest vibration energy efficiently in both horizontal and vertical directions.

The power output of the S-TENG achieves a maximum value when the excitation frequency is near resonant frequencies of the S-TENG structure.[28] Therefore, the electrical output of the S-TENG are measured when the shaker vibrates at natural resonant frequencies of the S-TENG, i.e., 16 Hz for vertical vibration and 8.5 Hz for horizontal vibration. As shown in Figure 4a, the average peak voltage increases linearly from 0 to 85 V with the vertical acceleration increasing from 0 to 23 m s^{-2} for vertical vibration resonance (16 Hz). At the same condition, the average peak current increased linearly from 0 to 5 μA, and the charge increases linearly from 0 to 35 nC with the vertical acceleration amplitude increasing from 0 to 23 m s^{-2} (Figure 4b,c). It is worth to noting that the dependence of the electrical signal on the acceleration suggests that the S-TENG can be used as a self-powered active acceleration sensor using a vertical vibrational mode. For horizontal vibration resonance (8.5 Hz), the average peak voltage, current, and charge increase as the horizontal acceleration increases from 0 to 15 m s^{-2}, and gradually approach their asymptotic values for a horizontal acceleration larger than 15 m s^{-2}. This implies that the separation distance and contact area between the elastomeric electrode and silicone rubber layer for the present S-TENG do not increase with an acceleration larger than 15 m s^{-2}. In addition, the instantaneous voltage, current, and charge measured under vertical

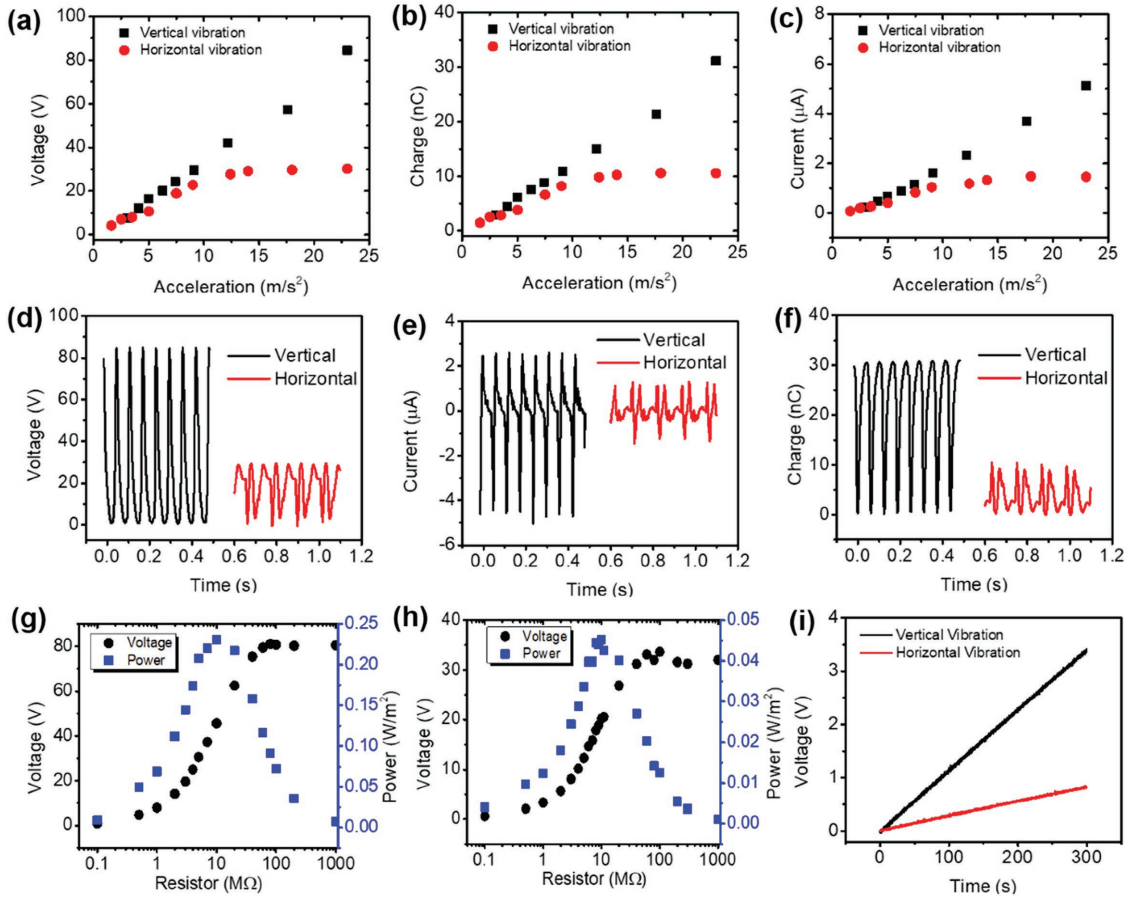

Figure 4. Electrical output of the S-TENG when the shaker vibrates at resonance frequencies of the S-TENG, i.e., 16 Hz for vertical vibration and 8.5 Hz for horizontal vibration. a) Average peak voltage, b) average peak current, and c) average peak charge as a function of the acceleration $|a| = 1–23$ m s^{-2}. d) Instantaneous voltage, e) current, and f) charge measured at $|a| = 23$ m s^{-2}; peak voltage and peak power as functions of the resistance power measured at $|a| = 23$ m s^{-2}. The power output of the S-TENG was measured under g) vertical resonance vibration and h) horizontal resonance vibration by using resistors as external loads. i) Charging voltage as a function of the charging time for a commercial capacitor of 50 μF.

and horizontal resonance vibration are shown in Figure 4d–f. Obviously, the electrical output of the S-TENG under vertical resonance vibration is higher than that of horizontal resonance vibration. This is due to the contact area between the silicone rubber layer and the electrode layer being larger under vertical vibration excitation as compared to horizontal vibration (Figure 1d,e).

The power output of the S-TENG was also investigated at the resonance frequency by using resistors as external loads. As shown in Figure 4 (g,h), the output voltage increases quickly as the resistance increases from 0.1 Ω to 100 MΩ, and then saturates when the resistance is further increased. As a result, the output power density is maximized at 240 mW m^{-2} with a load resistance of 10 MΩ under vertical resonance vibration with an acceleration amplitude of $|a| = 23$ m s^{-2}. Under horizontal vertical resonance vibration with the same acceleration, the output power density is maximized at 45 mW m^{-2} with a load resistance of 10 MΩ. It is worth to noting that the resistance at which the maximum power is produced decreases with the increase of frequency of current signal, as the triboelectric nanogenerator could be modeled as a capacitor, and ideally, the capacitor's resistance is modeled by $|R| = 1/(2\pi fC)$, with C being the capacitance of the S-TENG. The maximum power in Figure 2f is measured using a linear motor with frequency of 1 Hz, while in Figure 4g,h it is measured using a shaker under vertical vibration frequency of 16 Hz and horizontal vibration frequency of 8.5 Hz. As shown in Figure 1d,e and Figure S4 (Supporting Information), the frequency of a current signal measured under horizontal vibration is doubled compared to that measured under vertical vibration. Therefore, the maximum power is produced using a shaker at lower resistance than that measured using a linear motor, due to the increase of vibration frequency. In addition, the power density of TENGs highly depends on the triboelectric charge density. The output performance of the present S-TENG could be even higher (e.g., go to watt levels) by means of material improvement, structural optimization, surface modification, etc. For example, the contact surface could be further modified by adding micro/nanostructures, or the contact force can be increased by adding additional mass on top of the S-TENG, to increase the effective contact area.

Furthermore, Figure 4i shows the charging voltage as a function of the charging time using a commercial capacitor of 50 μF under vertical and horizontal resonance vibration with an acceleration amplitude of $|a| = 23$ m s^{-2}, respectively.

As demonstrated in Figure 4i, the S-TENG can harvest both vertical and horizontal vibration energy and charge a commercial capacitor. Additionally, the durability of the S-TENG is shown in Figure S5 (Supporting Information). The current output of the S-TENG is nearly constant for more than 30 000 cycles on a shaker under vertical vibration with a frequency of 16 Hz. This suggests that the S-TENG is robust.

2.3. Demonstration

Based on the performance of the S-TENG presented above, we find that the S-TENG is soft, robust, and capable of harvesting both vertical and horizontal vibration energy. Thus, it is an ideal candidate for vibration energy harvesting, and for a self-powered active acceleration sensor. **Figure 5**a shows the working circuit of a S-TENG for vibration energy harvesting as it is able to power a temperature and humidity sensor. The S-TENG was connected with a rectifier and a commercial capacitor for continuous direct outputs. Figure 5b shows a photo of the vibration energy harvesting system and the video for lighting light-emitting diodes (LEDs) is shown in Video S1 (Supporting Information). More than 20 LEDs were successfully lit up by placing the S-TENG on top of the model car. In addition, the humidity and temperature sensor was also successfully lit up after 300 s charging of the 100 µF capacitor. This indicates that our S-TENG has great potential application in harvesting vibration energy from vehicle vibration, building vibration, and vibration triggered by ocean waves, wind, and walking for sustainable energy sources.

In addition to energy harvesting, the S-TENG can also serve as a self-powered active sensor for vibration monitoring. According to Equations (1)–(3), the output signal of the S-TENG is sensitive to the dynamic process of the experienced mechanical disturbance, so it can work as a dynamic sensor to realize real-time monitoring of vibration acceleration and frequency. Figure 5d shows the block diagram of S-TENG for vibration sensing. As shown in the work of Yu et al.[21], the quantitative relationship of acceleration a, vibration frequency f, and output voltage V_{OC} can be determined as $a = bf^2 V_{OC}$. Here, b is a constant coefficient. From the real-time voltage signal of the S-TENG, the vibration frequency can be obtained using fast Fourier transform and the value of V_{OC} signal can also be easily obtained from the measured signal. For each vibration frequency f, there is a linear relationship between the voltage V_{OC} and acceleration a, i.e., $a = b_1 V_{OC}$. Here, $b_1 = bf^2$. Therefore, by submitting the real-time voltage V_{OC} to the relationship $a = b_1 V_{OC}$, the real-time acceleration a can be obtained. Figure 5e shows a photo of the self-powered car vibration acceleration sensor, which was realized by a live demonstration as shown in Video S2 (Supporting Information). The detailed comparison between the acceleration obtained from the S-TENG and a commercial accelerometer is shown in Figure 5f. The acceleration and frequency obtained from the S-TENG agrees well with that of the commercial accelerometer. Therefore, aside from harvesting vibration energy, our S-TENG can also serve as a self-powered vibration sensor.

3. Conclusion

In summary, a TENG based on the integration of spring and elastomer was designed. Along the cut surface of the elastomer-spring helical structure, a layer of conductive elastomer topped

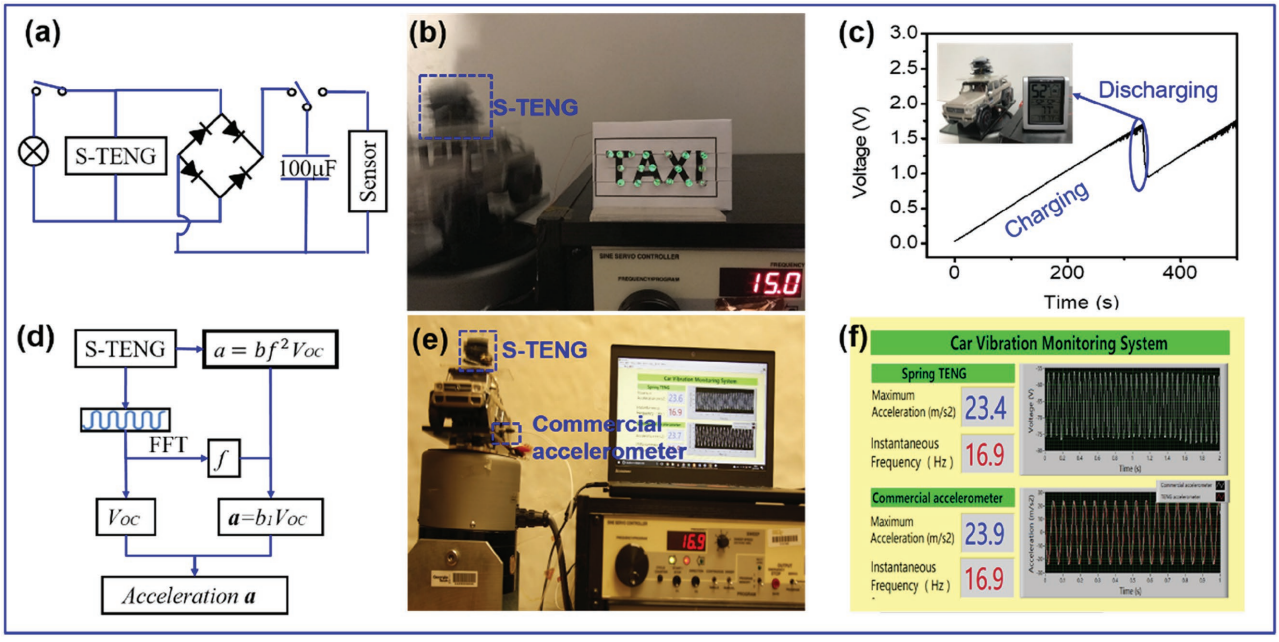

Figure 5. Applications of S-TENG for vibration energy harvesting and vibration sensing. a) The working circuit of S-TENG for vibration energy harvesting to power sensor and LEDs. b) Powering light-emitting diodes (LEDs) and c) humidity and temperature sensor with S-TENG on top of a model car using a shaker. d) The schematic diagram of S-TENG for acceleration sensing. e) Sensing the acceleration and frequency of the model car under vertical vibration excitation. f) Comparison of the S-TENG and commercial accelerometer.

the surface served as an electrode, and another layer of electrode was placed at the bottom of the helical structure surface covered by another layer of silicone rubber. With assistance of a spring and soft silicone rubber, the helical structure not only could vibrate vertically under vertical excitation but also could vibrate horizontally under horizontal excitation. Such vibration makes the distance in between a helical structure's adjacent surface change and form contact-separation mode TENG. Theoretical models are proposed for the two fundamental vibration modes, and the measured resonance frequency of the S-TENG agrees well with theoretical results and finite element simulation. Under vertical resonance vibration (16 Hz) and horizontal resonance vibration (8.5 Hz), the maximum average power density of the present S-TENG is found to be 240 and 45 mW m^{-2}, with a load of 10 MΩ and an acceleration amplitude of excitation being 23 m s^{-2}. The performance of S-TENG can be optimized by choosing proper materials or modifying surface morphology to increase its charge density, and by designing structure to enhance separation distance between the triboelectric layers. To tune the device to response to different resonant frequencies, the user could choose various springs with different stiffness, or thickness of silicone rubber, etc. Additionally, the dependence of output voltage of the S-TENG on acceleration and frequency indicates that it could be used as a self-powered active vibration sensor, which is demonstrated by a model car vibrating on a shaker. Therefore, our newly designed S-TENG has great potential application in harvesting arbitrary vibration energy, such as vehicle vibration, building vibration, and vibration triggered by ocean wave, wind, and walking. At the same time, it is also well suited for a self-powered vibration sensor.

4. Experimental Section

Fabrication of the S-TENG: Fabrication of S-TENG is shown in Figure S1 (Supporting Information). For the structural layers, the molds with acrylic sheets were manufactured by processing them into different parts on the laser cutter and gluing the parts together with epoxy. A spring was installed in the center of the box whose inner size is 3 cm × 3 cm × 6 cm (Figure S1a, Supporting Information). The liquid silicone rubber was obtained by mixing the silicone base and curing it with a volume ratio of 1:1 (Exoflex supersoft siliconee 0050 manufactured by Smooth-On, Inc.) in a beaker. The liquid silicone was then poured inside the mold with a spring installed in the center and cured at 40 °C for 6 h (Figure S1b, Supporting Information). The silicone between each spring coil was cut and removed to leave space for forming a helical contact-separation mode TENG (Figure S1c, Supporting Information). The elastomeric electrode layer of the S-TENG was prepared by first mixing the base and curing agent of silicone rubber (1:1, W/W) in a beaker, followed by blending carbon nanofiber (Pyrograf III carbon nanofiber PR-24-HT-HHT from Pyrograf Products Inc.) with the liquid silicone rubber (1:12, W/W). Next, the mixture was smeared over a flat acrylic sheet, and curved at 40 °C for 6 h. The resistance per unit length of the conductive elastomer is about 160 Ω cm^{-1} without any strain. Top and bottom electrode layers were adhered in series on the inner surfaces of the cut silicone base using Ecoflex 0050 as a glue. Finally, another silicone rubber layer was adhered on the surface of the top electrode layer (Figure S1d, Supporting Information).

Measurement of the Fabricated Devices: The carbon nanofiber added in to the electrode elastomeric was characterized by field emission scanning electron microscope (SU-8010, Hitachi). The elastomeric electrodes were connected to the Keithley 6514 electrometer to measure the electrical outputs including the open-circuit voltage, short-circuit current, and transferred charge. For the measurement of the electrical output capability of the S-TENG, external forces were applied by a commercial linear mechanical motor, which corresponded to the stretching and releasing operations, respectively. The applied force was measured by Vernier LabQuest Mini. During the measurement in Figures 3–5, the S-TENG was tested by putting the S-TENG on an electrodynamic shaker (Labworks ET-126 shaker) which works as an external vibration source generating a harmonic vibration with controlled amplitude and frequency along the vertical direction. To achieve the horizontal vibration, the shaker was rotated by 90°.

Supporting Information

Supporting Information is available from the Wiley Online Library or from the author.

Acknowledgements

M.X., P.W., and Y.-C.W. contributed equally to this work. The authors are grateful for the support received from the National Key Research and Development Program of China (Grant No. 2016YFA0202704), the "Thousands Talents" program for pioneer researcher and his innovation team in China, the National Natural Science Foundation of China (Grant Nos. 51506019, 61671017, 11672265, and 11621062), the Fundamental Research Funds for the Central Universities, China (Grant Nos. 3132016337 and 3132016204), the Young Elite Scientists Sponsorship Program by CAST (Grant No. 2016QNRC001). M.X., P.W., and C.Z. thank the China Scholarship Council for supporting research at the Georgia Institute of Technology.

Conflict of Interest

The authors declare no conflict of interest.

Keywords

elastomeric electrodes, mechanical energy harvesting, self-powered sensors, triboelectric nanogenerators, vibration energy harvesting

Received: September 4, 2017
Revised: October 4, 2017
Published online:

[1] Z. L. Wang, *Faraday Discuss.* **2015**, *176*, 447.
[2] Z. L. Wang, L. Lin, J. Chen, S. Niu, Y. Zi, *Triboelectric Nanogenerators*, Springer, Berlin, Germany **2016**.
[3] Z. L. Wang, *Mater. Today* **2017**, *20*, 74.
[4] Y. Zi, Z. L. Wang, *APL Mater.* **2017**, *5*, 074103.
[5] R. K. Gupta, Q. Shi, L. Dhakar, T. Wang, C. H. Heng, C. Lee, *Sci. Rep.* **2017**, *7*, 41396.
[6] Z. Quan, C. B. Han, T. Jiang, Z. L. Wang, *Adv. Energy Mater.* **2016**, *6*, 1501799.
[7] Z. L. Wang, J. Chen, L. Lin, *Energy Environ. Sci.* **2015**, *8*, 2250.
[8] J. Bae, J. Lee, S. Kim, J. Ha, B.-S. Lee, Y. Park, C. Choong, J.-B. Kim, Z. L. Wang, H.-Y. Kim, J.-J. Park, U. I. Chung, *Nat. Commun.* **2014**, *5*, 4929.
[9] K. Dong, J. Deng, Y. Zi, Y.-C. Wang, C. Xu, H. Zou, W. Ding, Y. Dai, B. Gu, B. Sun, Z. L. Wang, *Adv. Mater.* **2017**, *29*, 1702648.

[10] J. Wang, S. Li, F. Yi, Y. Zi, J. Lin, X. Wang, Y. Xu, Z. L. Wang, *Nat. Commun.* **2016**, *7*, 12744.
[11] J. Chen, Y. Huang, N. Zhang, H. Zou, R. Liu, C. Tao, X. Fan, Z. L. Wang, *Nat. Energy* **2016**, *1*, 16138.
[12] Z. L. Wang, T. Jiang, L. Xu, *Nano Energy* **2017**, *39*, 9.
[13] Z. L. Wang, *Nature* **2017**, *542*, 159.
[14] X. Pu, M. Liu, X. Chen, J. Sun, C. Du, Y. Zhang, J. Zhai, W. Hu, Z. L. Wang, *Sci. Adv.* **2017**, *3*, e1700015.
[15] R. D. I. G. Dharmasena, K. D. G. I. Jayawardena, C. A. Mills, J. H. B. Deane, J. V. Anguita, R. A. Dorey, S. R. P. Silva, *Energy Environ. Sci.* **2017**, *10*, 1801.
[16] C. Dagdeviren, Z. Li, Z. L. Wang, *Annu. Rev. Biomed. Eng.* **2017**, *19*, 85.
[17] A. C. Wang, C. Wu, D. Pisignano, Z. L. Wang, L. Persano, *J. Appl. Polym. Sci.* **2017**, *134*, 45674.
[18] K. Dong, Y.-C. Wang, J. Deng, Y. Dai, S. L. Zhang, H. Zou, B. Gu, B. Sun, Z. L. Wang, *ACS Nano* **2017**, *11*, 9490.
[19] S. L. Zhang, Y.-C. Lai, X. He, R. Liu, Y. Zi, Z. L. Wang, *Adv. Funct. Mater.* **2017**, *27*, 1606695.
[20] B. Zhang, L. Zhang, W. Deng, L. Jin, F. Chun, H. Pan, B. Gu, H. Zhang, Z. Lv, W. Yang, Z. L. Wang, *ACS Nano* **2017**, *11*, 7440.
[21] H. Yu, X. He, W. Ding, Y. Hu, D. Yang, S. Lu, C. Wu, H. Zou, R. Liu, C. Lu, Z. L. Wang, *Adv. Energy Mater.* **2017**, *7*, 1700565.
[22] M. Xu, Y.-C. Wang, S. L. Zhang, W. Ding, J. Cheng, X. He, P. Zhang, Z. Wang, X. Pan, Z. L. Wang, *Extreme Mech. Lett.* **2017**, *15*, 122.
[23] X. Cao, Y. Jie, N. Wang, Z. L. Wang, *Adv. Energy Mater.* **2016**, *6*, 1600665.
[24] W. Li, D. Torres, R. Díaz, Z. Wang, C. Wu, C. Wang, Z. Lin Wang, N. Sepúlveda, *Nat. Commun.* **2017**, *8*, 15310.
[25] Q. Jing, Y. Xie, G. Zhu, R. P. Han, Z. L. Wang, *Nat. Commun.* **2015**, *6*, 8031.
[26] W. Xu, L.-B. Huang, M.-C. Wong, L. Chen, G. Bai, J. Hao, *Adv. Energy Mater.* **2017**, *7*, 1601529.
[27] P.-K. Yang, Z.-H. Lin, K. C. Pradel, L. Lin, X. Li, X. Wen, J.-H. He, Z. L. Wang, *ACS Nano* **2015**, *9*, 901.
[28] Y. Hu, J. Yang, Q. Jing, S. Niu, W. Wu, Z. L. Wang, *ACS Nano* **2013**, *7*, 10424.
[29] C. Wu, R. Liu, J. Wang, Y. Zi, L. Lin, Z. L. Wang, *Nano Energy* **2017**, *32*, 287.
[30] T. Jiang, Y. Yao, L. Xu, L. Zhang, T. Xiao, Z. L. Wang, *Nano Energy* **2017**, *31*, 560.
[31] S. Niu, Z. L. Wang, *Nano Energy* **2015**, *14*, 161.
[32] M.-L. Seol, J.-W. Han, D.-I. Moon, M. Meyyappan, *Nano Energy* **2017**, *32*, 408.
[33] H. Liu, C. Lee, T. Kobayashi, C. J. Tay, C. Quan, *Smart Mater. Struct.* **2012**, *21*, 035005.
[34] T. L. Schmitz, K. S. Smith, *Mechanical Vibrations: Modeling and Measurement*, Springer Science & Business Media, Berlin, Germany **2011**.

